ple, the quantity $k_{\mathrm{obs}}/[\mathrm{CH_4}]$ (k_{obs}, observed rate) was not affected by the total pressure under conditions in which the total pressure was >10 torr. These relatively complex molecules relax somewhat more efficiently than Group VI metal carbonyls: Compare with P. L. Bogdan, J. R. Wells, E. Weitz, *ibid.* **113**, 1294 (1991).
11. E. O. Fischer and K. Bittler, *Z. Naturforsch. B* **16**, 225 (1961).
12. A. J. Rest, I. Whitwell, W. A. G. Graham, J. K. Hoyano, A. D. McMaster, *J. Chem. Soc. Chem. Commun.* **1984**, 624 (1984); *J. Chem. Soc. Dalton Trans.* **1987**, 1181 (1987); D. M. Haddleton, *J. Organomet. Chem.* **311**, C21 (1986); R. R. Andrea, H. Luyten, M. A. Vuurman, D. J. Stufkens, A. Oskam, *Appl. Spectrosc.* **40**, 1184 (1986); R. R. Andrea, M. A. Vuurman, D. J. Stufkens, A. Oskam, *Recl. Trav. Chim. Pays-Bas* **105**, 372 (1986).
13. D. M. Haddleton and R. N. Perutz, *J. Chem. Soc. Chem. Commun.* **1985**, 1372 (1985); ______, S. A. Jackson, R. K. Upmacis, M. Poliakoff, *J. Organomet. Chem.* **311**, C15 (1986); S. T. Belt *et al.*, *J. Chem. Soc. Chem. Commun.* **1987**, 1347 (1987); S. B. Duckett *et al.*, *Organometallics* **7**, 1526 (1988).
14. S. T. Belt, F. W. Grevels, W. E. Klotzbuecher, A. McCamley, R. N. Perutz, *J. Am. Chem. Soc.* **111**, 8373 (1989).
15. Greater rates were seen when CO was present.
16. C. E. Brown, Y. Ishikawa, P. A. Hackett, D. M. Rayner, *J. Am. Chem. Soc.* **112**, 2530 (1990); see also Y. Ishikawa, C. E. Brown, P. A. Hackett, D. M. Rayner, *Chem. Phys. Lett.* **150**, 506 (1988).
17. Other workers also find that binding energies for charge-neutral metal-alkane complexes lie in this range. See, for example, G. K. Yang, K. S. Peters, V. Vaida, *Chem. Phys. Lett.* **125**, 566 (1986); J. K. Klassen, M. Selke, A. A. Sorensen, *J. Am. Chem. Soc.* **112**, 1267 (1990).
18. For studies of the rate of vibrational relaxation of coordinatively unsaturated metal carbonyls in solution, see M. Lee and C. B. Harris, *J. Am. Chem. Soc.* **111**, 8963 (1990); S.-C. Yu, R. Lingle, Jr., J. B. Hopkins, *ibid.* **112**, 3668 (1990).
19. For reviews, see G. J. Kubas, *Acc. Chem. Res.* **21**, 120 (1988); *Comments Inorg. Chem.* **7**, 17 (1988).

20. Supported by the Director of the Office of Energy Sciences, Chemical Sciences Division, of the U.S. Department of Energy under contract DE-AC03-76SF00098.

7 August 1991; accepted 17 October 1991

Oxygen Supersaturation in Ice-Covered Antarctic Lakes: Biological Versus Physical Contributions

H. CRAIG, R. A. WHARTON, JR., C. P. MCKAY

Freezing in ice-covered lakes causes dissolved gases to become supersaturated while at the same time removing gases trapped in the ablating ice cover. Analysis of N_2, O_2, and Ar in bubbles from Lake Hoare ice shows that, while O_2 is ~2.4 times supersaturated in the water below the ice, only 11% of the O_2 input to this lake is due to biological activity: 89% of the O_2 is derived from meltwater inflow. Trapped bubbles in a subliming ice cover provide a natural "fluxmeter" for gas exchange: in Lake Hoare as much as 70% of the total gas loss may occur by advection through the ice cover, including ~75% of the N_2, ~59% of the O_2, and ~57% of the Ar losses. The remaining gas fractions are removed by respiration at the lower boundary (O_2) and by molecular exchange with the atmosphere in the peripheral summer moat around the ice.

LAKE HOARE IS ONE OF A NUMBER of ice-covered polar lakes in the Dry Valley Region of southern Victoria Land, Antarctica (*1*) that exist by the grace of two special and regional features: (i) the Transantarctic Mountain Range that blocks the flow of ice from the polar plateau and at the same time effectively eliminates precipitation, and (ii) the very low mean air temperature (~−20°C) that provides permanent ice covers 3 to 6 m thick, sheltering "warm-water" (~0°C) lakes over a region of some 5000 km^2. These lakes lie on the land like a series of Szilardian chemostats, fed by glacial meltwaters of varying nutrient contents and hosting rich benthic and planktonic microflora, all thriving on the unique substandard ecologies of low-light, near-freezing, highly oxygenated waters while shielded by ice from the Antarctic rigors. The uniqueness of these ecological characteristics and of the mechanisms of atmospheric gas exchange and high supersaturation of the water make these Antarctic lakes interesting for studies of both terrestrial and possible early Martian habitats (*2, 3*).

Lake Hoare (*2*) is an elongate (4.1 by 1.0 km), shallow (maximum and mean depths: 34 and 14.2 m) lake at the eastern end of Taylor Valley, fed during austral summer by melt streams from Suess Glacier and Lake Chad. The perennial ice cover, ~5 m thick at the time of our work, melts along the marges during summers to provide a moat ~3 m wide that receives the inflowing water: water is removed entirely by sublimation and ablation of the ice cover and evaporation from the moat (moat area is ~2% of total lake area). The lake water is highly supersaturated in O_2 and N_2, and Wharton *et al.* (*2, 3*) originally proposed that freezing of the lake water produces the N_2 supersaturation but that biological production is the major source for supersaturation of O_2. In this report we show how measurements of N_2 and Ar can be used to evaluate the physical and biological effects responsible for supersaturation of O_2 and the removal rates of gases from lakes by ice convection. This approach is an extension of methods used to evaluate O_2 supersaturation effects in the North Pacific gyres (*4*).

The concentration of dissolved O_2 (Fig. 1) is very high in the well-mixed layer below the ice-water interface, averaging 2.4 times saturation relative to atmospheric solubility: below this layer O_2 decreases rapidly to zero in the bottom water (*2*). O_2 is supplied to the lake by inflowing summer meltwater and by photosynthesis below the ice and is removed by (i) ablation and sublimation of ice containing trapped air bubbles, (ii) respiration, and (iii) molecular exchange in the summer moat around the ice cover. Between these sources and sinks two processes are interposed: enrichment of the dissolved O_2 concentration by the formation of ice at the lake surface, and downward transport of O_2 by diffusion to a respiration sink (algal mats) on the bottom. The O_2 sources have been estimated only indirectly: Wharton *et al.* (*2*) used the sedimentation rate of carbon in a nearby lake and an estimate of the O_2 supplied by stream input to calculate that 69% of the net input of O_2 is due to biological production. These authors (*3*) also used the N_2 and O_2 saturation ratios to calculate the proportions of biological to physical O_2 production: that method gave the fraction of biological input as 68% (*5*). We show, however, that those estimates are an order of magnitude too high because of the use of N_2, rather than Ar, as a surrogate inert gas for O_2.

We analyzed the gases in bubbles trapped in the ice cover. Our measurements were made on vertically oriented elongate bubbles near the upper surface of a block of ice collected during the 1987–1988 field season. Bubbles from three pieces were analyzed by gas chromatography (GC) (*4*) for N_2, O_2, and Ar after crushing and extraction of gases in vacuum (*6*). The results are set out in Table 1.

The most striking observation is that the gases do not resemble air: they are depleted in N_2 and enriched in O_2 and Ar, so that the composition is much more similar to that of dissolved gases in water. The bubble compositions are reasonably uniform, and all values lie between air and solubility compositions. The N_2/Ar ratios are intermediate between that of air (83.6) and that of saturated water at 0°C (37.0), as expected for partitioning of gases between bubbles and water when gas exsolution is occurring as a result of removal of water by freezing. The

---

H. Craig, Isotope Laboratory, Scripps Institution of Oceanography, University of California at San Diego, La Jolla, CA 92093.
R. A. Wharton, Jr., Desert Research Institute, University of Nevada System, Reno, NV 89506.
C. P. McKay, Space Science Division, National Aeronautics and Space Administration Ames Research Center, Moffett Field, CA 94035.

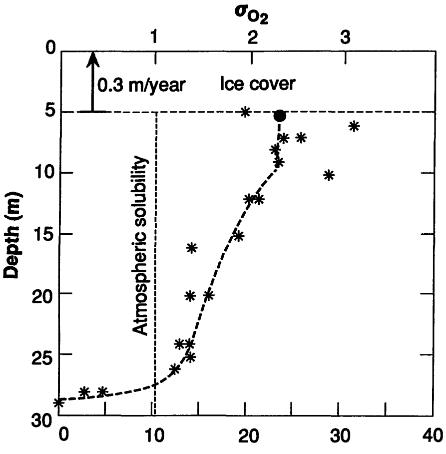

Fig. 1. Dissolved O_2 concentrations during the austral summer of 1982–1983 in Lake Hoare, below the 5-m-thick perennial ice cover (*2*). The observed concentrations (stars) range from zero at the bottom, where respiration in microbial mats consumes all the O_2, to 2.4 (± 0.4) times the equilibrium atmospheric solubility of 10.2 cm^3 (STP)/kg at the ice-water interface where photosynthesis is occurring in a 4-m-thick mixed layer. The solid point is the calculated concentration at the interface based on the measured composition of gas bubbles in the ice. The arrow shows the vertical advection of ice due to removal by sublimation and ablation (*2*).

O_2/Ar ratios in the bubbles, however, are greater than either the air or solubility ratios, and this must be due to botany. The mean O_2/Ar ratio (the C1 value, 23.86) is 6.4% greater than the ratio in air (22.43) and fully 16.2% greater than the ratio in atmospheric dissolved gases (20.53). Evaluation of the biological production of O_2 therefore requires a model of the freezing and exsolution effects to provide a baseline O_2/Ar ratio for comparison. We used the N_2/Ar ratios to model the compositional variations during bubble formation and then compared the measured and calculated O_2/Ar ratios to assess the biological contribution.

During freezing, gases become supersaturated in the region immediately below the newly forming ice, until a bubble nucleates and forms a gas phase. As freezing proceeds, gas is transferred from solution to the bubble, until finally the bubble is sealed off and moves toward the upper surface with its encapsulating ice, where it is removed by ablation. The supersaturated water left behind is mixed back into the lake water with its residual dissolved gases. The two-phase gas distribution during the freezing process is given by

$$C_i^0 = X_i^G \cdot P_G \cdot F_L (\beta_i + \psi) \qquad (1)$$

where X_i^G is the mole or volume fraction of gas i in the bubble at the ambient pressure P_G, and β_i is its Bunsen solubility coefficient (*7*). The original gas concentration in the water before freezing begins is C_i^0, and F_L is the mass fraction of liquid water remaining at any stage, relative to the initial mass of water from which ice has been extracted (*7*).

Equation 1 gives the material balance of gas i between solution and bubble during two-phase partitioning as ice is extracted and the bubble grows. Gas and solution are assumed to remain in dynamic equilibrium until the bubble is sealed and the residual water is mixed away. The progress variable ψ scales the gas-to-fluid ratio during the separation: ψ is actually the ratio of the bubble volume V_G at P_G to the mass of liquid water M_L remaining at any stage of the freezing process. Thus the product $\psi \cdot P_G \cdot F_L$ is the ratio of the total gas in the bubble at standard temperature and pressure (STP) to the initial mass of fluid M_L^0. Because this product is the same for all gases, the N_2/Ar and O_2/Ar ratios along the two-phase trajectory are defined by the initial ratios, the β_i values, and ψ as in Eq. 1. The bubble trajectory for a system with initial concentrations equal to the atmospheric equilibrium values is shown in the upper left (gas-phase) part of Fig. 2. The value of ψ for the measured N_2/Ar ratios (Table 1), given by the mean N_2/Ar ratio (sample C1), is 71 cm^3 (at P_G) per kilogram of residual fluid. This corresponds to a bubble 5 mm in diameter for each cubic centimeter of coexisting liquid.

Figure 2 also shows (upper right curve) the gas-phase trajectory for an O_2-enriched system with the ratios observed in the bubbles, in which the O_2 enrichment in the water took place before the onset of freezing. This trajectory is simply offset from that of the original system by a constant enrichment of the O_2/Ar ratio; that is, the total O_2 in the system (the left side of Eq. 1) is

$$C^0_{O_2} = C^*_{O_2} + J \qquad (2)$$

when the initial concentration in the water is the atmospheric equilibrium solubility (C^*). Here J, the O_2 added by photosynthesis, is given directly by the offset of the O_2/Ar ratio in the bubbles (~23.9) from the ratio on the equilibrium (J = 0) curve (21.3), measured at the N_2/Ar ratio (48.7) in the bubbles. At this point the O_2/Ar ratio has been increased by a factor of 1.12 relative to the abiogenic system, and the fraction of the total O_2 derived from biological processes is the difference in O_2/Ar ratios: that is 1 − (21.3/23.9) = 0.11. Thus, we find that photosynthesis in the lake produces only 11% of the total O_2.

In general, O_2 production by photosynthesis may be continuous during the freezing process, so that there are a large number of possible trajectories between the two described above. One such trajectory, in which the O_2 production has simply been taken as proportional to ψ, is shown in Fig. 2 (curve 3) and is given by

$$C^0_{O_2} = C^*_{O_2} [1 + (J_{max}/C^*_{O_2}) (\psi/\psi_{max})] \qquad (3)$$

where J_{max} is the total amount of O_2 produced at the final stage of freezing when $\psi = \psi_{max}$ and the bubble is sealed off and has the same value as the constant J in Eq. 2. A detailed study of bubble-gas ratios should allow the determination of the variability of such trajectories over the time span provided by the 5 m of ice cover (~17 years).

Equation 1 can also be used to calculate removal rates of gases by ice convection for any assumed values of the initial concentrations C_i^0. The ice thickness, ~5 m, defines P_G = 1.45 atm: F_L is then 0.20 for ψ = 71, corresponding to freezing out 80% of the water in the original fluid volume, for the assumption of equilibrium (1 atm) solubility concentrations in the entering meltwater. The total gas volume in bubbles is $\psi \cdot P_G \cdot F$ = 20.6 cm^3 (STP) per kilogram of original fluid: these bubbles are in equilibrium with 9.8 cm^3 (STP) of gas dissolved in the 0.2 kg of residual fluid and having the individual concentrations in row 8 of Table 1. The

Table 1. Compositions of N_2, O_2, and Ar and ratios in gas bubbles trapped in a block of the Lake Hoare ice cover, compared with atmospheric and dissolved gas compositions. Rows 2, 3, and 4 give the compositions measured on occluded gas bubbles (*5*). Row 5 gives the composition of dissolved gases in fresh water at 0°C. Rows 6 and 7 give the Bunsen solubility coefficients and the atmospheric equilibrium solubilities in water at 0°C, in units of cm^3 (STP)/kg, based on the Weiss solubility equations (*10*). Row 8 gives the calculated gas concentrations, in cm^3 (STP)/kg, in the residual liquid phase (RL) in equilibrium with the gas in bubbles (C1) at the ambient pressure P_G.

Sample	N_2	O_2	Ar	N_2/Ar	O_2/Ar
Air (%)	78.084	20.946	0.934	83.60	22.426
A1 (%)	66.72	31.91	1.36	48.99	23.43
A2 (%)	65.25	33.35	1.39	46.79	23.92
C1 (%)	66.20	32.44	1.36	48.69	23.86
Water, 0°C (%)	63.22	35.07	1.71	37.00	20.53
β ($\times 10^3$)	23.74	49.10	53.64	0.443	0.915
C^* (0°C)	18.43	10.22	0.498	37.00	20.53
C (RL)	22.79	23.10	1.06	21.55	21.84

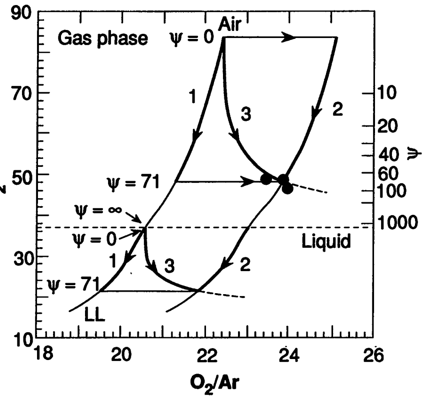

Fig. 2. Gas and liquid-phase trajectories for N_2/Ar and O_2/Ar ratios during single-stage transfer of gases from solution to bubbles during freezing. The first bubbles have ratios equal to the "air" point ($\psi = 0$): as freezing proceeds and gas is transferred to the bubbles, the gas phase moves down the trajectory to the limiting value of the initial water phase at infinite ψ. Similarly, the remaining dissolved gases in the liquid phase move down the lower trajectory to the limiting minimum ratios in the last liquid (at LL). A horizontal arrow marks the N_2/Ar ratio in the bubbles (at $\psi = 71$) when they became isolated from the liquid by occlusion in the ice. Trajectory 1 is for a system with no O_2 production (Eq. 1): the bubble gases (solid points) fall to the right of this curve because of addition of O_2 by photosynthesis (O_2 depletion would produce points to the left of the curve). Trajectory 2 describes a system with an initial excess O_2 content due to production before the freezing process (Eq. 2). Trajectory 3 shows the general case in which O_2 production takes place during the freezing interval, in this case at a rate proportional to the freezing rate (Eq. 3). Regardless of the actual trajectory, the biological O_2 production is measured by the offset of the bubble coordinates from the inorganic trajectory, at the value of the progress variable ψ fixed by the measured N_2/Ar ratios (*11*).

liquid-phase N_2/Ar and O_2/Ar ratios (7) define the curves in the lower space of Fig. 2 for the equilibrium and O_2-enriched systems, offset in O_2/Ar ratio by the same factor of 1.12.

In this model ~68% of the total gas input (meltwater plus photosynthesis) is removed from the lake in the ice layer. The fraction of each component in the trapped gas phase in the ice is given (from Eq. 1) by $[\psi/(\psi + \beta_i)]$: 75% of the N_2, 59% of the O_2, and 75% of the Ar from an original element of meltwater are in bubbles in the ice when 80% of the water has been frozen, and these fractions are removed with the upward advection of the ice cover and its loss by ablation and sublimation. The remaining fractions of the gases are removed by downward mixing and respiration for O_2 and by molecular exchange with the atmosphere in the narrow summer moat around the ice cover for all gases.

These fractional losses by ice convection are a function of the initial concentrations in the volume elements in which freezing occurs. In the above calculations freezing occurs in the entering meltwater, which is thought (*3, 8*) to flow in beneath the ice cover unmixed with the supersaturated lake water, and the initial values of Eq. 1 are taken as the atmospheric solubilities. If the initial concentrations are higher because of mixing with ambient lake water, the freezing trajectories in Fig. 2 start farther down the curves (at lower gas ratios), and the values of ψ are smaller at the observed gas ratios in the bubbles. Thus, if we assume that $C^0{}_N = 20$ cm^3 (STP) for N_2, for which the freezing trajectory would start at $N_2/Ar = 66$ rather than at 83.6, the observed bubble ratios are reached at $\psi = 21$ instead of 71, and the fraction of original N_2 in the ice bubbles is reduced from 75 to 47%. A further complication in the freezing model is that the fraction of residual liquid F_L must also be frozen at some stage or be removed through subsurface flow, in order to balance the influx of meltwater if a steady state is assumed. Because the meltwater input occurs only in summer and because there are no data on the total gas content of the ice cover, a complete model of the freezing process cannot be made at present, and the fractional gas losses by ice convection must be taken as upper limits. However, the O_2 loss in ice calculated from the meltwater model (~59%) is in reasonable agreement with the value of ~48% obtained for the fractional retention of O_2 in laboratory-grown columnar ice and Arctic flows (*9*).

The meltwater-freezing model with initial saturation values is also in reasonable agreement with observed gas concentrations in the lake water. The calculated concentrations in the residual liquid (Table 1) give saturation values of $\sigma_N = 1.23$, $\sigma_O = 2.25$, and $\sigma_{Ar} = 2.11$. The N_2 and O_2 values obtained from the bubble analyses are similar to the values recorded at the ice/water interface [(*3*); compare with (*5*)]: that is, 1.31 and 1.97, respectively, and the O_2 value matches the lake profile quite well (Fig. 1). The O_2 saturation should be similar to, but slightly less than, the value for Ar because of the very similar β values: the slightly higher saturation for O_2 is due to the biological input. From these saturation values it is clear why the use of N_2/O_2 ratios (*3*) gives a much larger biological input for O_2 (68% versus 11%). The N_2/O_2 balance equation used in (*3*) requires $\sigma_N = \sigma_{Ar}$ [compare (*5*)], because either gas can be used in the equation, in which all losses for abiogenic gases are assumed to be proportional to the solubilities. However, this is not the case when freezing and bubble removal in ice are important. Because the O_2/N_2 ratios vary by factors of 2 in both phases, the use of N_2 as a surrogate for O_2 results in large errors. On the other hand, the O_2/Ar ratios are almost invariant for nonbiological effects.

The primary result of this study, that ~11% of the O_2 input to the lake is due to photosynthesis, depends only on the O_2/Ar ratios and should therefore be correct to a few percent. The presence of a permanent ice cover implies that this result is an approximate yearly average, although the winter freezing of inflowing meltwater should result in seasonal variations. Despite the uncertainties in the fractional gas losses by ice convection, it is clear that 40 to 70% of the O_2 input to Lake Hoare is removed by occlusion and advection in the ice cover. Our results show that loss of gases by way of bubbles trapped in ice can be the major gas-removal process in closed lakes at high latitudes or altitudes. The treatment given here applies to all lakes with a winter ice cover that traps gas bubbles, but in order to study the gas exchange rates properly one also needs to measure absolute gas concentrations in the ice cover and in the surface water of the open moat.

REFERENCES AND NOTES

1. D. G. Ball and R. L. Nichols, *Geol. Soc. Am. Bull.* 71, 1703 (1960); W. Green and E. I. Friedman, Eds., *Lakes of the McMurdo Dry Valleys* (Antarctic Research Series, American Geophysical Union, Washington, DC, in press).
2. R. A. Wharton, C. P. McKay, G. M. Simmons, B. C. Parker, *Limnol. Oceanogr.* 31, 437 (1986).
3. R. A. Wharton *et al.*, *Nature* 325, 343 (1987).
4. H. Craig and T. Hayward, *Science* 235, 199 (1987).
5. The fraction of O_2 input by biology, from equations 1 and 2 in (*3*), is: $A_O/(A_O + B_O) = (\sigma_N - 1)/(\sigma_O - 1)$, where A is the nonbiological source (the product of the input water flux and the atmospheric-equilibrium gas concentration C^*), B is the net biological input (zero for N_2), σ is the saturation value, defined as the ratio of actual concentration, C, to C^*, and subscripts N and O denote N_2 and O_2. This equation results from cancellation of the concentration terms and gas loss coefficients in equations 1 and 2. In the text of (*3*) and in table 1 (column 2: rows 2 and 3) the N_2 saturation values σ_N are given incorrectly as 1.45 and 1.63. The correct values are 1.31 and 1.49. Using $\sigma_N = 1.63$ (at 12 m depth) in the above equation, one obtains the biological input fraction given by the authors: using the correct value of 1.49 (with $\sigma_O = 2.55$) one obtains the ratio $B_O/(A_O + B_O) = 68\%$ as the fraction of total O_2 input due to biological production. The flaw in this calculation is the assumption that the "net loss coefficients" for N_2 and O_2 are equal, that is, that the concentration ratio of these gases is changed only by biological effects and is unaffected by physical processes such as freezing.
6. Three pieces containing bubbles were cut from an original block 23 by 13 cm in section, sampled from between depths of 1 and 2 m in the ice cover, well below the summer thaw regime. Ice crystal morphology showed that meltwater percolation had not interacted with bubbles in the samples. Two adjacent pieces, A1 and A2, were taken from the uppermost 10 cm: the third piece, C1, was cut from the lowermost 15 cm. Given the rate of ice loss by sublimation and ablation as ~30 cm/year (*2*), the bubbles we used were ~16 years old, with A1 + A2 older than C1 by ~10 months. All samples were ~12 cm long with elongate bubbles that were fully enclosed in the ice and did not channel to longer

bubbles exposed at either surface. Two methods were used for vacuum extraction of the gases. Samples A1 and A2 were cracked open by thermal stress from an external hot-air blast: in sample C2 the gas was removed by partial melting and ultrasonic extraction from the meltwater. The gas contents of the three ~100-g pieces were ~1.2, 1.1, and 0.64 cm^3 (STP), but, because these pieces were cut to exclude bubbles in long channels open to air, we collected only a fraction of the original gas in each piece of ice. The GC techniques and analytical precision are described in note 14 of (*4*).

7. In Eq. 1, C_i^0, the initial gas content of a kilogram of water, is partitioned during the freezing process between gas and liquid phases by the equilibrium condition: $C_i = \beta_i \cdot p_i$, where C_i is the concentration in the liquid and p_i is the partial pressure of gas i in the bubbles, given by $X_i \cdot P_G$. The two terms on the right side of Eq. 1 are therefore the amounts of gas i in solution and in bubbles, expressed in cubic centimeters at standard temperature and pressure (cm^3 STP) per kilogram of original fluid. Because only ratios are plotted in Fig. 2, all equilibrium abiogenic systems should follow the gas and liquid trajectories given by these curves (except for slight deviations due to mixing): however, waters that have been partially outgassed or mixed with supersaturated waters will produce bubbles that begin on the curve somewhere below the initial "air point" and arrive at a given composition with lower values of ψ and larger values of F_L than in the case of initial saturation equilibrium. Nevertheless, the biogenic systems will follow parallel trajectories, offset to higher O_2/Ar ratios by displacements proportional to the input of O_2 by net biological production.
8. C. P. McKay *et al.*, *Nature* **313**, 561 (1985).
9. Z. Top, S. Martin, P. Becker, *Geophys. Res. Lett.* **12**, 821 (1985).
10. R. F. Weiss, *Deep-Sea Res.* **17**, 721 (1970).
11. Trajectories 1 and 2 in Fig. 2 can be described in terms of an initial mass of 1 kg of meltwater with $C^*_{O_2}$ = 10.22 cm^3 (STP), (σ_O = 1) at the ψ = 0 point. On curve 1 the mass of water is reduced by freezing to 200 g of liquid water containing 4.10 cm^3 (STP) of O_2, with σ_O = 2.00. Photosynthesis (*J*) then produces 0.50 cm^3 of additional O_2, or 11% of the total O_2 content of the water, with a final σ_O = 2.25. Trajectory 2 follows an addition of 1.23 cm^3 (STP) of photosynthetic O_2 to the original 1 kg of water and 10.22 cm^3 of atmospheric O_2, so that the biologic fraction is again 11% of the total dissolved O_2. Freezing along curve 2 then produces 200 g of residual water, with 4.60 cm^3 of O_2 and σ_O = 2.25. All other trajectories (for example, curve 3) produce a similar final state of the system.
12. We thank D. Burtner for the GC measurements; D. Andersen, L. Leary, and D. Schwindler for field assistance to R.A.W. and C.P.M.; and E. Hernandez for maintaining the Isotope Laboratory at Scripps Institution of Oceanography (SIO). Work at SIO was supported by NSF grant DPP87-22718 and National Aeronautics and Space Administration (NASA) grant NAGW-972. Work at the Desert Research Institute and Ames Research Center was supported by NSF grant DPP84-16340 and NASA grant NCA2-182.

28 October 1991; accepted 30 October 1991

The Earth's Angular Momentum Budget on Subseasonal Time Scales

J. O. DICKEY, S. L. MARCUS, J. A. STEPPE, R. HIDE

Irregular length of day (*LOD*) fluctuations on time scales of less than a few years are largely produced by atmospheric torques on the underlying planet. Significant coherence is found between the respective time series of *LOD* and atmospheric angular momentum (*AAM*) determinations at periods down to 8 days, with lack of coherence at shorter periods caused by the declining signal-to-measurement noise ratios of both data types. Refinements to the currently accepted model of tidal Earth rotation variations are required, incorporating in particular the nonequilibrium effect of the oceans. The remaining discrepancies between *LOD* and *AAM* in the 100- to 10-day period range may be due to either a common error in the *AAM* data sets from different meteorological centers, or another component of the angular momentum budget.

THE ROTATION VECTOR $\mathbf{\Omega}(t)$ OF THE solid Earth (where t denotes time and solid Earth refers to the crust and the mantle) with which the solid Earth rotates relative to a frame of reference defined by the fixed stars exhibits complicated changes of up to several parts in 10^8 in speed, corresponding to variations of several milliseconds in the length of day (*LOD*), $\Lambda(t)$. These changes occur over a broad spectrum of time scales and are manifestations of (i) changes in the inertia tensor of the solid Earth associated with redistribution of matter within it, and (ii) the action of applied torques. These torques are primarily produced by gravitational action of the moon, sun, and planets and by motions in the underlying liquid core and overlying oceans and atmosphere (*1*).

Irregular *LOD* fluctuations on time scales less than a few years are largely produced by atmospheric torques (*1–5*); concomitant stresses on the solid Earth are applied directly over continental regions and indirectly over the oceans. If the angular momentum of the solid Earth is $\mathbf{H}^{(s)}$ and $\mathbf{L}$ is the applied torque, then $\dot{\mathbf{H}}^{(s)}$, the time rate of change of $\mathbf{H}^{(s)}$ in an inertial frame satisfies

$$\dot{\mathbf{H}}^{(s)} = \mathbf{L} \qquad (1)$$

It is convenient to write

$$\mathbf{L} = -\dot{\mathbf{H}}^{(a)} + \mathbf{l} \qquad (2a)$$

and

$$\mathbf{l} = \mathbf{l}_{ext} - \dot{\mathbf{H}}^{(o)} - \dot{\mathbf{H}}^{(c)} \qquad (2b)$$

where $\mathbf{H}^{(a)}$ is the total angular momentum of the atmosphere, so that $\mathbf{l}$ is the difference between (i) torques acting upon the whole Earth associated with external gravitational effects ($\mathbf{l}_{ext}$) and (ii) torques associated with angular momentum fluctuations in the oceans [$\dot{\mathbf{H}}^{(o)}$] and core [$\dot{\mathbf{H}}^{(c)}$]. The angular momentum budget between the atmosphere and solid Earth is then

$$\dot{\mathbf{H}}^{(s)} = -\dot{\mathbf{H}}^{(a)} + \mathbf{l} \qquad (3)$$

Investigations into the Earth's angular momentum budget and research into solid Earth-atmosphere interactions have been revolutionized by the advent of modern space geodetic measurements of the Earth's rotation. These advances have been accompanied by improvements in measurements and numerical models of the Earth's global atmosphere, which are used to calculate the atmospheric angular momentum (*AAM*). The most progress has been made in investigations concerned with the axial component of Eq. 3, in which *LOD* fluctuations reflecting changes in the axial component $H_3^{(s)}$ of $\mathbf{H}^{(s)}$ are compared with fluctuations in the axial component $H_3^{(a)}$ of $\mathbf{H}^{(a)}$ (Fig. 1).

The present paper extends these studies down to periods of a few days, thereby improving the limits that can be placed on the magnitude of l_3 on these time scales. A nonzero value of l_3 greater than the errors involved in its determination would be a measure of the extent to which angular momentum fluctuations in other components of the system (such as the oceans) have to be taken into account at these high frequencies (assuming that external gravitational effects are properly accounted for). Hence, a comparison between *AAM* and *LOD* at these higher frequencies could uncover the ocean's role and further elucidate our understanding of the interaction between the solid Earth and the atmosphere.

The observed *LOD* time series can conveniently be separated into four components (*2*): (i) a constant term Λ_0 = 86,400 s representing the standard length-of-day, (ii) strictly periodic

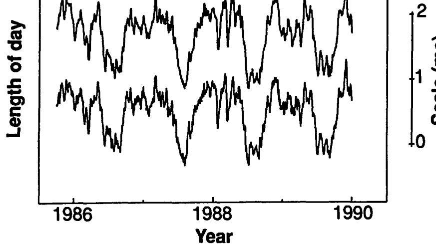

Fig. 1. Time series of LOD*, as determined by the Kalman-filtered combined space geodetic data (top) and from the combined *AAM* data (bottom); a 1-year moving average has been removed from both series. Tidal terms (*18*) have been removed from *LOD*.

J. O. Dickey, S. L. Marcus, J. A. Steppe, Jet Propulsion Laboratory, California Institute of Technology, 4800 Oak Grove Drive, Pasadena, CA 91109.
R. Hide, Robert Hooke Institute, The Observatory, Clarendon Laboratory, Parks Road, Oxford OX1 3PU, England, U.K.